 doi:10.20944/preprints202207.0073.v1

Article

Biocompatibility of ceramic materials in $CaO-P_2O_5$ system, obtained via heat treatment of cement-salt stone

Otabek Toshev [1,*] https://orcid.org/0000-0003-3513-3383, **Tatiana Safronova** [1, 2], https://orcid.org/0000-0002-9799-5029 **Maksim Kaimonov** [1] https://orcid.org/0000-0002-4970-2092, **Tatiana Shatalova** [1, 2], https://orcid.org/0000-0002-4304-8624, **Elena Klimashina** [2], **Yulia Lukina** [3], https://orcid.org/0000-0003-0121-1232 **and Konstantin Malyutin** [4], https://orcid.org/0000-0002-1824-1086

[1] Department of Materials Science, Lomonosov Moscow State University, Building, 73, Leninskie Gory, 1, 119991 Moscow, Russia; safronovatv@my.msu.ru (Tatiana Safronova); shatalovatb@gmail.com (Tatiana Shatalova)

[2] Department of Chemistry, Lomonosov Moscow State University, Building, 3, Leninskie Gory, 1, 119991 Moscow, Russia

[3] National Medical Research Center for Traumatology and Orthopedics named after N.N. Priorov, Priorova 10, 127299 Moscow, Russia

[4] Skolkovo Institute of Science and Technology, Bolshoy boulevard 30, 121205 Moscow, Russia

* Correspondence: otabektoshev0995@gmail.com; Tel.: +7-977-522-50-62

Abstract: Biocompatibility of ceramic materials in $CaO-P_2O_5$ system was investigated using different methods, including in vitro and in vivo tests. Ceramics based on calcium pyrophosphate $Ca_2P_2O_7$ were obtained by annealing cement-salt stone from highly concentrated hardening suspensions (HCHS). Cement-salt stone was prepared using powder mixtures of calcium citrate tetrahydrate $Ca_3(C_6H_5O_7)_2{\cdot}4H_2O$ and monocalcium phosphate monohydrate (MCPM) $Ca(H_2PO_4)_2{\cdot}H_2O$. These salts were mixed with each other in such a way that calcium pyrophosphate and calcium polyphosphate were present in the final ceramic product in the following weight ratios: $Ca(PO_3)_2/Ca_2P_2O_7$ = 0/100; 5/95; 10/90 and 20/80. Distilled water was added to a homogenized powder mixtures of $Ca_3(C_6H_5O_7)_2{\cdot}4H_2O$ and $Ca(H_2PO_4)_2{\cdot}H_2O$ by a water/solid ratio of 0,5 by weight. The obtained suspensions were shaped using silicon molds and left to dry in air for a week. The phase composition of the obtained samples of cement-salt stone was represented by brushite $CaHPO_4{\cdot}2H_2O$, monetite $CaHPO_4$, calcium citrate tetrahydrate $Ca_3(C_6H_5O_7)_2{\cdot}4H_2O$ and monocalcium phosphate monohydrate $Ca(H_2PO_4)_2{\cdot}H_2O$. According to the XRD data, the phase composition of ceramic materials after annealing in the temperature range of 800-1000 ^{0}C was mainly represented by the β-$Ca_2P_2O_7$ phase. In vivo tests shown that obtained ceramic materials can be recommended for regenerative treatments for bone defects.

Keywords: calcium pyrophosphate, calcium polyphosphate, biocompatibility, bone implants, regenerative medicine

1. Introduction

Calcium phosphate ceramic materials are widely used in regenerative medicine for the treatment or replacement damaged bone tissue due to their excellent biocompatibility [1-3]. Materials, which are used in regenerative medicine must be resorbable. Despite the great progress in the development of ceramic materials based on calcium phosphates, nowadays increasing resorbability of the biomaterials is one of the main challenges of materials science.

One of the main inorganic components of human bone tissue is hydroxyapatite $Ca_{10}(PO_4)_6(OH)_2$ Ca/P=1,67, which is a low-rate resorbable material. Synchronization of the rate of material resorption and the rate of growth of new bone tissue is required to enhance the bone regeneration process.

In this regard, the key characteristic of the material is its ability to resorb in the environment of the body. To increase resorbability of ceramic materials, the concept of using

 doi:10.20944/preprints202207.0073.v1

calcium pyrophosphate $Ca_2P_2O_7$ and calcium polyphosphates $Ca(PO_3)_2$ has been developed. Generally, these materials, that have a Ca to P ratio of 1 and 0.5 correspondingly, which are lower than that of hydroxyapatite $Ca_{10}(PO_4)_6(OH)_2$ possess increased resorbability [4, 5]. Therefore, ceramics based on calcium phosphates with a low Ca/P ratio are of huge scientific interest for designing materials for bone implants. [6-12].

Ceramics based on $Ca_2P_2O_7$ were obtained by applying direct powder precursors [13]. Direct precursors are calcium phosphate, which have the Ca/P ratio equal to the ratio of ceramic phase [13]. Such precursors are brushite ($CaHPO_4 \bullet 2H_2O$) [14 ,15], monetite ($CaHPO_4$) [16, 17], γ-$Ca_2P_2O_7$ [18] and β-$Ca_2P_2O_7$ [19]. There are also indirect precursors, which are a mixture of calcium phosphates with a ratio of Ca/P=1. In this case, the formation of the $Ca_2P_2O_7$ phase is observed at the stage of heat treatment of a ceramic material, which is associated with the heterophase reaction between the starting substances and the products of their thermal conversion [20]. Ceramics based on $Ca_2P_2O_7$ are annealed at temperatures above 1150°C [21, 22]. The addition of a lower melting phase of $Ca(PO_3)_2$ can significantly reduce the annealing temperature. Depending on the annealing temperature, various polymorphic modifications of $Ca_2P_2O_7$ can be obtained: amorphous calcium pyrophosphate - at 450 °C; γ- $Ca_2P_2O_7$ - at 530 °C, β - $Ca_2P_2O_7$ at 700 – 750 °C, α - $Ca_2P_2O_7$ at 1140-1179 °C [23].

Calcium polyphosphate can be obtained by polycondensation of the MCPM $Ca(H_2PO_4)_2 \bullet H_2O$:

$$nCa(H_2PO_4)_2 \cdot H_2O \rightarrow (Ca(PO_3)_2)n$$

In the temperature range of 690-750 °C γ - $Ca(PO_3)_2$ transforms into the β - $Ca(PO_3)_2$, but at temperatures above 750 °C the β – modification transforms into the α – modification [24].

The main aim of this work was to investigation of biocompatibility of ceramics based on calcium pyrophosphate $Ca_2P_2O_7$ and calcium polyphosphate $Ca(PO_3)_2$ using in vitro and in vivo tests. The ceramic materials were obtained by annealing cement-salt stone formed from highly concentrated hardening suspensions including calcium citrate tetrahydrate $Ca_3(C_6H_5O_7)_2 \bullet 4H_2O$ and monocalcium phosphate monohydrate $Ca(H_2PO_4)_2 \bullet H_2O$. The phase composition and microstructure of the materials were investigated using X-Ray diffraction analysis and scanning electron microscopy. The obtained materials showed good resorption in the simulated body fluid (SBF) and in vivo model mediums.

2. Materials and Methods

2.1. Initial reagents and synthesis

Calcium citrate tetrahydrate $Ca_3(C_6H_5O_7)_2 \cdot 4H_2O$ (CAS No. 5785-44-4, puriss. p.a. ≥85%) and monocalcium phosphate monohydrate $Ca(H_2PO_4)_2 \cdot H_2O$ (CAS No. 10031-30-8, puriss. 99%) for synthesis of ceramic materials were purchased from Sigma Aldrich.

2.2. Preparation of the calcium pyrophosphate and calcium polyphosphate ceramics

A highly concentrated aqueous suspension was obtained by mixing calcium citrate and MCPM powders. These salts were mixed with each other in a such way that calcium pyrophosphate and calcium polyphosphate were present in the final ceramic product in the following ratios: $Ca(PO_3)_2/Ca_2P_2O_7$ = 0/100; 5/95; 10/90 and 20/80 (Table 1). The amount of the used calcium citrate and monocalcium phosphate monohydrate were calculated according to the following reaction:

$$Ca_3(C_6H_5O_7)_2 \cdot 4H_2O + 3\ Ca(H_2PO_4)_2 \cdot H_2O + 5H_2O \rightarrow 6CaHPO_4 \cdot 2H_2O + 2H_3C_6H_5O_7 \quad (1)$$

Ceramic based on pyrophosphate and calcium polyphosphate was obtained by molding and subsequent annealing of brushite cement stone at a temperature range 800 - 1000°C for 3 hours.

2.3. Characterization

Preprints (www.preprints.org) | NOT PEER-REVIEWED | Posted: 5 July 2022 doi:10.20944/preprints202207.0073.v1

X-Ray diffraction (XRD) analysis was conducted using a Rigaku D/Max-2500 (Rigaku, Japan).

The microstructure of the ceramic materials was studied using a LEO SUPRA 50VP (Carl Zeiss, Germany) scanning electron microscope (SEM) with an acceleration voltage of 21 kV. The images were recorded using Everhart-Thornley secondary electron detector.

The microstructure of the surface of obtained ceramics was investigated using a Nikon ECLIPSE E600 P04 optical microscope.

2.3.1. Determination of plastic strength

Cone penetrometric method [25] was applied to determine the plastic strength of the obtained composites. A Rebinder conical plastometer was used for measuring plastic strength. The plastic strength of the system was calculated by the formula:

$$R = \frac{L}{l} \cdot k \cdot \frac{F}{h^2} \quad (1)$$

where R – plastic strength [MPa], L/l – plastometer shoulders ratio (length in cm), k – dimensionless coefficient, which depends from angular opening of cone.

$$k = \frac{\cos^2 \frac{\alpha}{2} ctg \frac{\alpha}{2}}{\pi} \quad (2)$$

$\alpha = 60^o$, k = 0,413.

2.3.2.Determination of strength properties

To determine the strength characteristics the obtained ceramics, balks with characteristic sizes of 10x10x30 mm were formed from cement dough. The water/solid ratio was 0,5 for cements based on calcium citrate and monocalcium phosphate monohydrate. The resulting cement dough was mixed in a teflon porcelain bowl for 30 seconds.

The bending and compressive strengths of samples were determined using universal testing machines LFV 10-T50 (Switzerland) and P-05.

2.3.3. Determination of true density

Density of the materials/samples was determined via pycnometric method. Density of the materials was estimated using formula (3):

$$\rho = \frac{(m_1 - m_2) \cdot \rho(\kappa)}{(m_2 - m_1) + (m_4 - m_3)} \quad (3)$$

where m_1 - the weight of empty pycnometer [g]; m_2 - the weight of pycnometer with powder [g]; m_3 - the weight of pycnometer with powder and liquid [g]; m_4 - the weight of pycnometer with liquid [g]; ρ (κ) – the density of kerosene [g/cm3].

2.3.4. Thermal analysis

Thermal analysis (TA) was carried out on a NETZSCH STA 409 PC Luxx thermal analyzer (NETZSCH, Germany). Heating rate was 10oC/min, temperature range was 20-1000°C. The weight of the samples for measurements was about 10 mg. The composition of the gas phase formed upon decomposition of samples was studied using a QMS 403C Aëolos quadrupole mass spectrometer (NETZSCH, Germany) coupled to the NETZSCH STA 409 PC Luxx thermal analyzer. Mass spectra (MS) were recorded for m/z 18 (H_2O), as well as for m/z 44 (CO_2).

2.3.5. pH – measurements

The study of ion activity in solutions (pH) was carried out using a multichannel ion meter Econix-Expert-001 (Russia) equipped with a glass electrode. Calibration of the electrodes was conducted using solutions with known concentrations of the ions and standard buffer solutions with a given pH.

pH - measurements were performed at room temperature (25°C) for one day at a powder/water mass ratio of 1/125. The data were recorded every 1 s.

2.3.6. In vivo tests

 doi:10.20944/preprints202207.0073.v1

The animal study protocol was approved by the Institutional Review Board (or Ethics Committee) of National Medical Research Center for Traumatology and Orthopedics named after N.N. Priorov, Ministry of Health of the Russian Federation (protocol code 005, date of approval 12.05.2021). The methods used in the work comply with the approved ISO 10993 standards; among them ISO 10993-2-2009 (Animal welfare requirements); ISO 10993-5-2011 (Tests for in vitro cytotoxicity); ISO 10993-6-2021 (Tests for local effects after implantation).

In vivo tests were performed using a model of subcutaneous implantation on Wistar rats. Preclinical assessment of biocompatibility, resorption and antibacterial effect of the obtained calcium phosphate matrices were carried out in vivo on five male Wistar rats weighing 250-300 g using a model of ectopic osteogenesis. Histological examination of morphological changes was studied using standard light microscopy, phase contrast and polarization microscopy in a Leica DM 4000 B LED microscope with a Leica DFC 7000 T camera. Thin sections were stained with hematoxylin and eosin. As a part of the histological study, a morphometric analysis of the revealed morphological signs was carried out by the method of semi-quantitative scoring. The signs were assessed using a five-point system. The presence of macrophages, fibroblasts, lymph-macrogaphal infiltration was assessed on a scale:

4 - no sign;
3 - weakly expressed sign;
2 - moderately pronounced sign;
1 - a well-defined sign;
0 - the most pronounced sign

Fibrous capsule maturity, thickness and vascularization on a scale:

0 - no sign;
1 - weakly expressed sign;
2 - moderately pronounced sign;
3 - a well-defined sign;
4 - the most pronounced sign.

Biocompatibility was assessed by summing the average scores for each trait in each sample in the group.

3. Results and discussion

XRD patterns of the cement stone based on calcium citrate and MCPM are shown in **Fig. 1.**

Preprints (www.preprints.org) | NOT PEER-REVIEWED | Posted: 5 July 2022 doi:10.20944/preprints202207.0073.v1

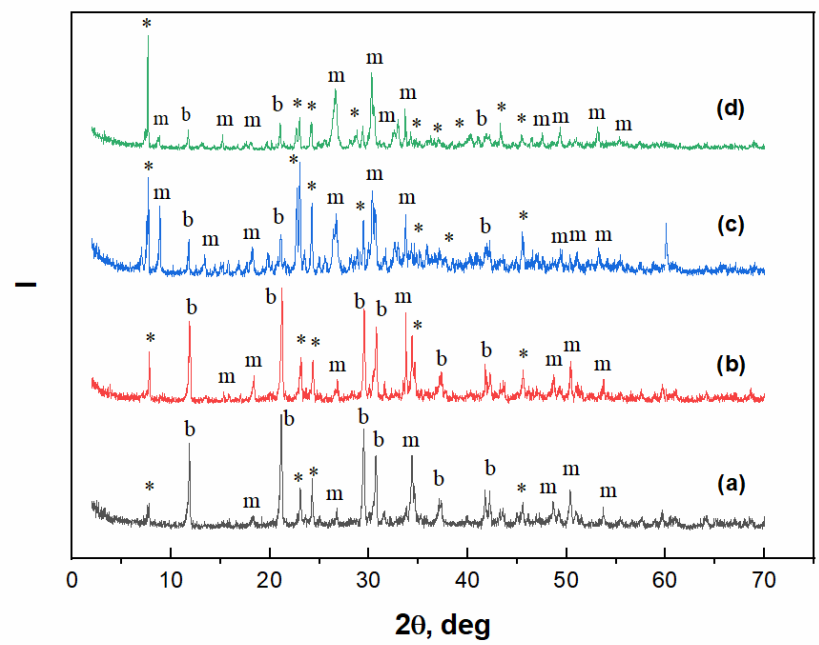

* – $Ca(H_2PO_4)_2 \bullet H_2O$ (PDF 9-347); b – $CaHPO_4 \bullet 2H_2O$ (PDF 72-713);
m – $CaHPO_4$ (PDF 75-1520).

Fig. 1. XRD spectra of the cement stone obtained from calcium citrate tetrahydrate and MCPM mixture with weight ratio of: a) $Ca(PO_3)_2/Ca_2P_2O_7$ = 0/100; b) $Ca(PO_3)_2/Ca_2P_2O_7$ = 5/95, c) $Ca(PO_3)_2/Ca_2P_2O_7$ = 10/90, d) $Ca(PO_3)_2/Ca_2P_2O_7$ = 20/80.

According to XRD data, the phase composition of cement stone with different ratios of MCPM to calcium citrate (**Fig. 1**) is represented by: brushite, monetite and unreacted MCPM phases. Increasing the MCPM to calcium citrate molar ratio leads to an increase in monetite phase and a decrease in brushite phase, as can be determined by the intensity of the corresponding XRD peaks. The increase in monetite content is associated with its higher thermodynamic stability at lower pH values [26], which is due to an increase in the amount of MCPM in the composition of the cement mixture.

Cement stone formed at a $Ca(PO_3)_2/Ca_2P_2O_7$ ratio of 0/100 has thick rod-like crystals with a small amount of lamellar structure. (**Fig. 2**).

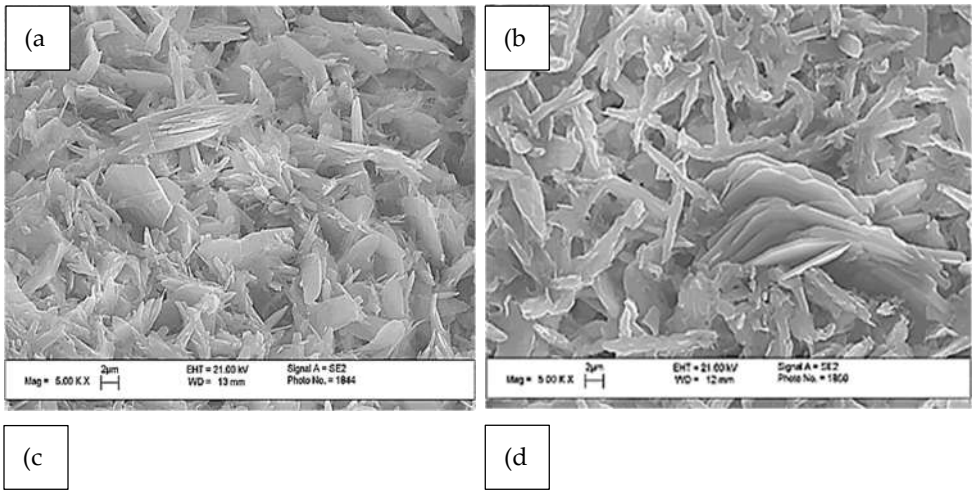

Preprints (www.preprints.org) | NOT PEER-REVIEWED | Posted: 5 July 2022 doi:10.20944/preprints202207.0073.v1

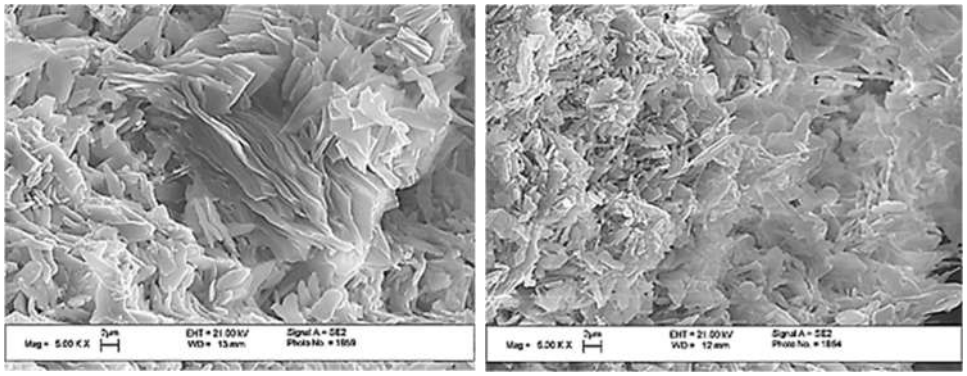

Fig. 2. SEM images of cement stone, with weight ratio of: a) $Ca(PO_3)_2/Ca_2P_2O_7 = 0/100$; b) $Ca(PO_3)_2/Ca_2P_2O_7 = 5/95$, c) $Ca(PO_3)_2/Ca_2P_2O_7 = 10/90$, d) $Ca(PO_3)_2/Ca_2P_2O_7 = 20/80$.

An increase in the MCPM content in initial mixture leads to an increase in the content of thin, lamellar crystals of different sizes, which is most likely associated with the conditions of supersaturation and rapid formation of crystals of the newly formed phases. The cement stone obtained from the initial mixture composition of 20/80 has smaller crystalline size as compared to other compositions.

Fig. 3 represents the dependence of the plastic strength on time for different components of mixtures of calcium citrate and MCPM.

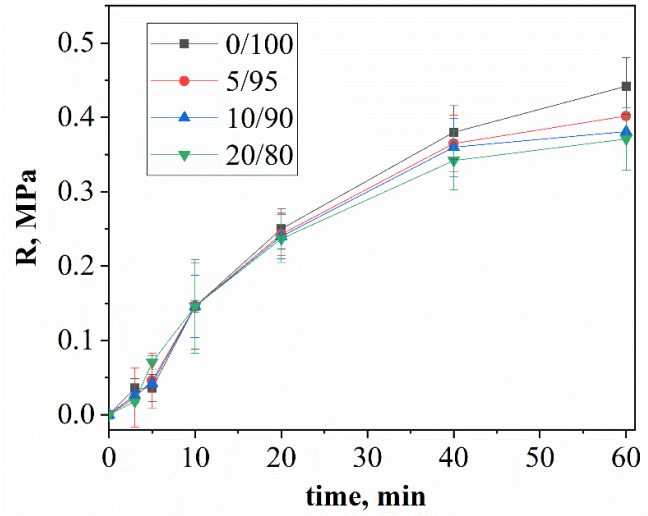

Fig. 3. The time dependence of plastic strength of cement stone, with weight ratio of: a) $Ca(PO_3)_2/Ca_2P_2O_7 = 0/100$; b) $Ca(PO_3)_2/Ca_2P_2O_7 = 5/95$, c) $Ca(PO_3)_2/Ca_2P_2O_7 = 10/90$, d) $Ca(PO_3)_2/Ca_2P_2O_7 = 20/80$.

The increasing of plastic strength is associated with the process of hardening of cement solutions and formation of cement stone. In the first 10 minutes after mixing the cement pastes the plastic strength increases faster for compositions, containing high volume MCPM. The rate of brushite formation at this stage is limited by the rate of dissolution of calcium citrate, which increases with an excess of acidic MCPM. Further the change in plastic strength is different for different compositions: the plastic strength is inversely proportional to the concentration of MCPM in the initial mixtures. Plastic strength depends on the rate of formation of cement stone and the adhesion strength between the newly formed crystals: an increase in the amount of MCPM in the initial mixture leads to a decrease in the proportion of brushite with lamellar crystals in the final product, which form smaller contacts with each other and, accordingly, results in a low plastic strength.

Preprints (www.preprints.org) | NOT PEER-REVIEWED | Posted: 5 July 2022 doi:10.20944/preprints202207.0073.v1

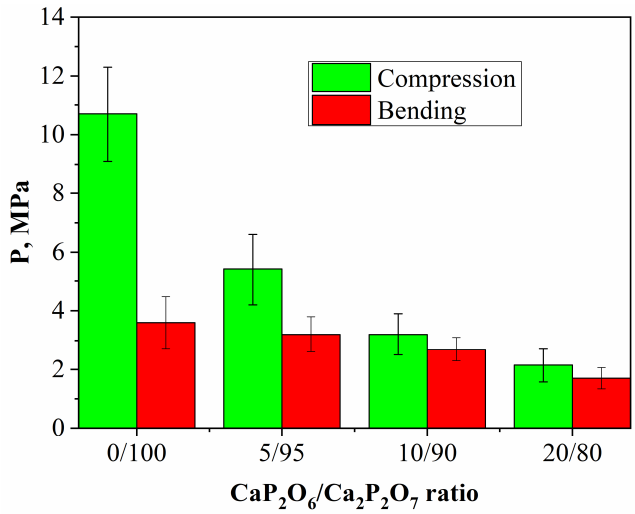

Fig. 4. Compressive and bending strengths of cement stone with weight ratio of: a) $Ca(PO_3)_2/Ca_2P_2O_7$=0/100; b) $Ca(PO_3)_2/Ca_2P_2O_7$=5/95, c) $Ca(PO_3)_2/Ca_2P_2O_7$=10/90, d) $Ca(PO_3)_2/Ca_2P_2O_7$=20/80.

The mechanical strength of cement stone is inversely proportional to the concentration of MCPM in the initial cement mixture, which is associated with a decrease in the amount of the final product (brushite) per unit volume with an increase in MCPM (**Fig. 4**). This is due to the presence of lamellar crystals and their less cohesion with each other.

The true density of cement stone decreases in all series from 0/100 to 20/80 (**Fig. 5**), which is associated with the presence of MCPM in initial composition.

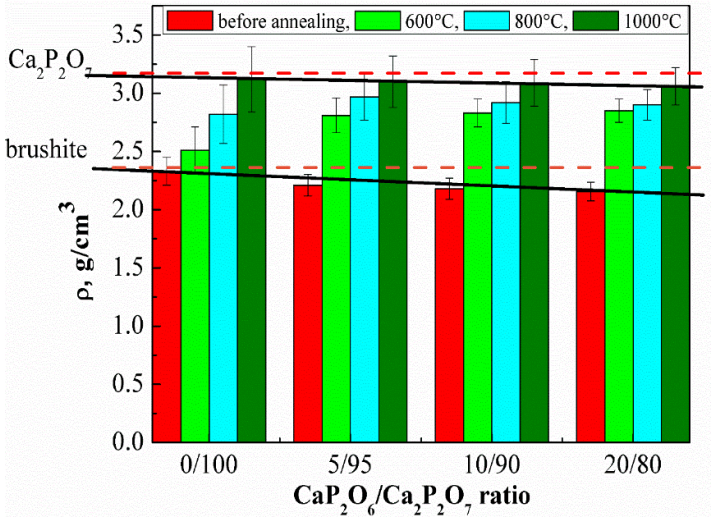

Fig. 5. True density of the ceramic materials before and after annealing in the temperature range of 600-1000 °C.

Dashed lines on the graph show the value of true density for brushite (ϱ=2,33 g/cm3) [27]. Solid lines show the value from our experiments. As seen in fig.6, increasing annealing temperature leads to increasing the true density of cement stone, which is associated with the recrystallization and formation of calcium pyrophosphate and polyphosphate. According to the literature, the true density of calcium pyrophosphate and calcium polyphosphate are 3,09 and 2,82 g/cm3, respectively [28, 29]. A more intense increase of the true density under the influence of temperature is characteristic for the compositions with a high MCPM content due to the formation of a lower-melting phase of calcium polyphosphate, which intensifies the sintering process.

Preprints (www.preprints.org) | NOT PEER-REVIEWED | Posted: 5 July 2022 doi:10.20944/preprints202207.0073.v1

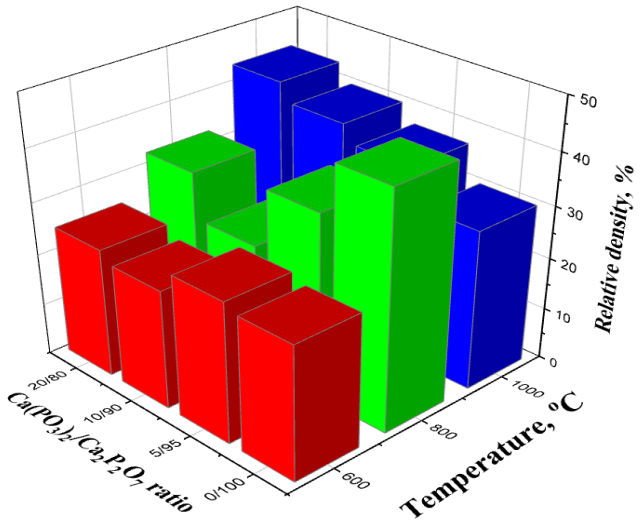

Fig. 6. Relative density of samples with weight ratio of: a) $Ca(PO_3)_2/Ca_2P_2O_7$ = 0/100; b) $Ca(PO_3)_2/Ca_2P_2O_7$ = 5/95, c) $Ca(PO_3)_2/Ca_2P_2O_7$ = 10/90, d) $Ca(PO_3)_2/Ca_2P_2O_7$ = 20/80 annealed in the temperature range of 600-1000 °C

The relative density of ceramic materials increases with increasing annealing temperature, reaching 43,7% at 1000°C (**Fig. 6**). For bulk samples increase of relative density is negligible above 500°C, which is associated with weight loss.

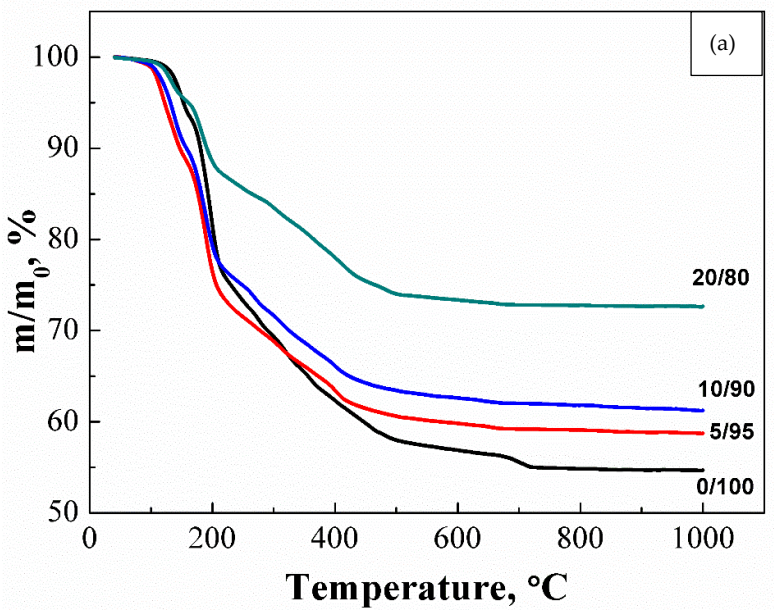

Preprints (www.preprints.org) | NOT PEER-REVIEWED | Posted: 5 July 2022 doi:10.20944/preprints202207.0073.v1

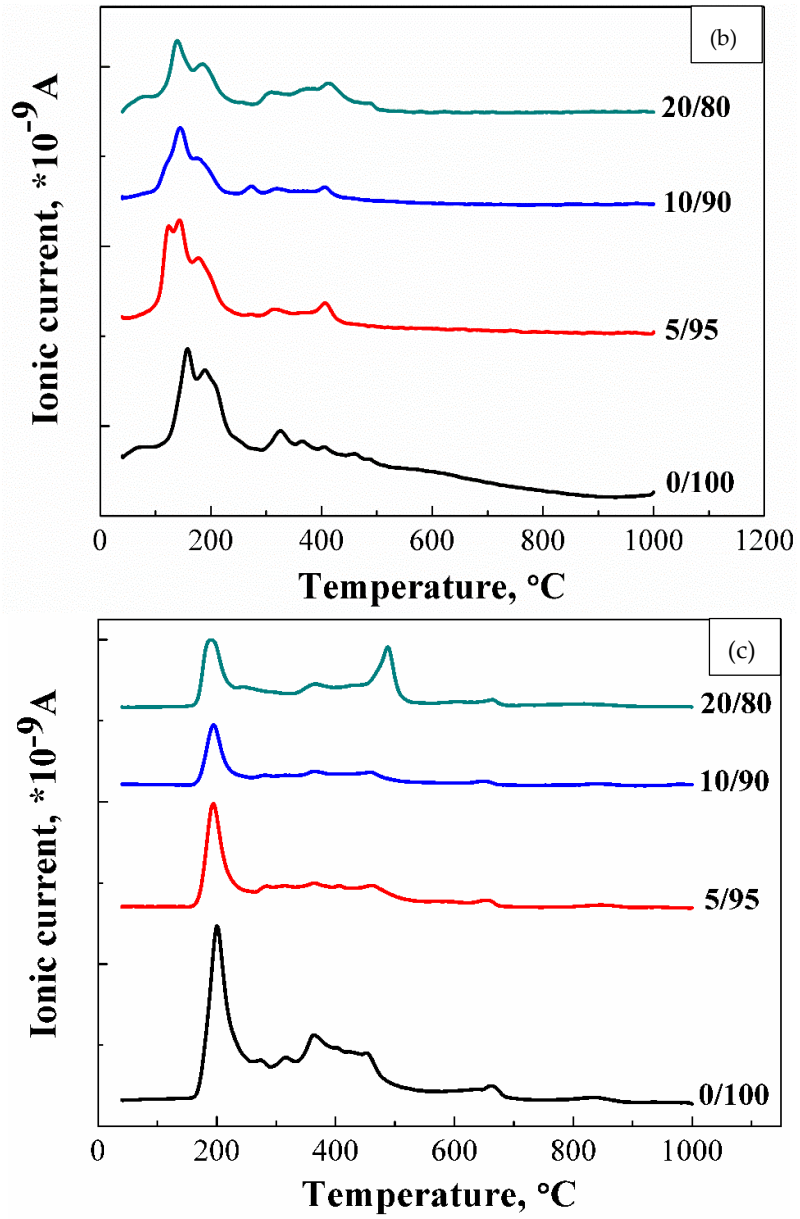

Fig. 7. Thermal analysis of synthesized brushite powders from calcium citrate and MCPM: a) powder mass versus temperature upon heating; b, c) ion current curves according to mass spectroscopy for m/Z=18 (H_2O) (b) and for m/Z=44 (CO_2) (c) respectively.

Thermal analysis of the obtained samples is shown in **Fig. 7**: temperature dependence of the mass of formed samples (**Fig. 7 a**), temperature dependence of ion current for water m/Z=18 (H_2O) (**Fig. 7 b**), and carbon dioxide m/Z=44 (CO_2) (**Fig. 7 c**). The mass loss curve for sample 0/100 contains steps characteristic of brushite, namely the conversion of brushite to monetite (~ 200°C), and then monetite to pyrophosphate (~ 400°C). The presence of unreacted starting components in the samples (a component taken in excess) and the accompanying reaction products determine the presence of additional steps of mass loss and peaks on the curves of the dependence of the ion current on temperature (**Fig. 7 b, c**). The curves of the dependences of the ion current for water (MS, m/Z = 18) for samples 0/100, 5/95, 10/90, and 20/80 is shown on the **Fig. 7 b**. In this graph, peaks of CO_2 can be seen in the range of 160 - 250°C, the presence of which can be attributed to the decomposition of the co-product of the reaction of the formation of brushite - citric acid ($t_{decom.}$ =

Preprints (www.preprints.org) | NOT PEER-REVIEWED | Posted: 5 July 2022 doi:10.20944/preprints202207.0073.v1

175°C). The intensity of this peak increases with increasing content of MCPM in the composition of the initial mixture. The excess of this initial component, apparently, contributes to a more complete reaction (1), which leads to the formation of a large amount of citric acid.

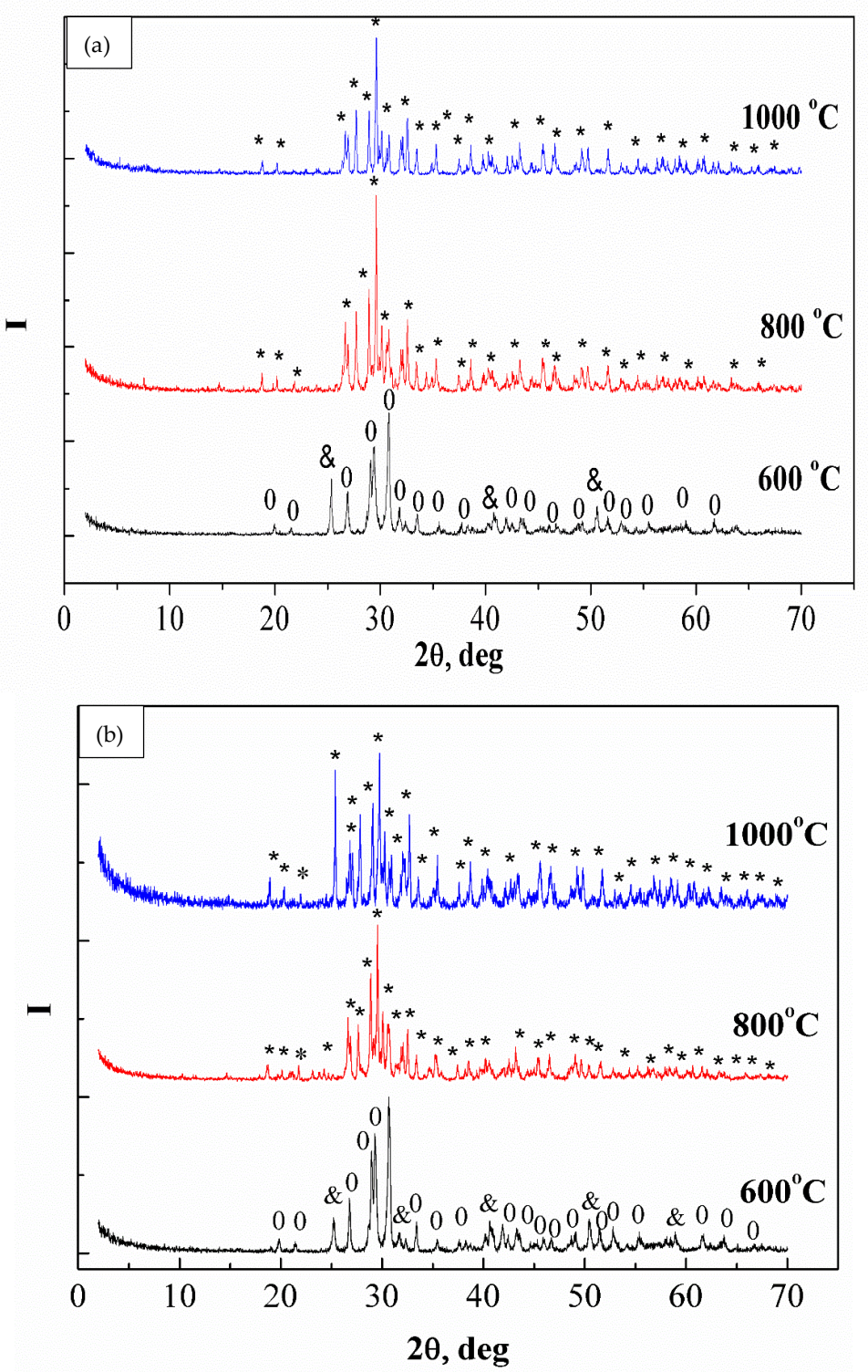

* - β-$Ca_2P_2O_7$ (PDF 9-346); 0 – γ- $Ca_2P_2O_7$ (PDF 17-499); & - β-$Ca(PO_3)_2$ (PDF 17-500)

Fig. 8. XRD of ceramic materials with weight ratio of: a) $Ca(PO_3)_2/Ca_2P_2O_7$=0/100; b) $Ca(PO_3)_2/Ca_2P_2O_7$=20/80 in the temperature range of 600-1000 °C

Preprints (www.preprints.org) | NOT PEER-REVIEWED | Posted: 5 July 2022 doi:10.20944/preprints202207.0073.v1

The phase composition of ceramic materials 0/100 и 20/80, obtained by annealing the cement stone based on $Ca_3(C_6H_5O_7)_2 \bullet 4H_2O$ and $Ca(H_2PO_4)_2 \bullet H_2O$, is consistent with the data of true density (**Fig. 8 a** and **Fig. 8 b**) respectively. After annealing at the temperature of 600°C, a calcium polyphosphate phase is observed in all compositions. When the temperature increases to 1000°C, calcium polyphosphate transforms to calcium pyrophosphate. This is due to the thermal decomposition of $Ca(PO_3)_2$ at temperatures above 900 °C to calcium pyrophosphate according to the equation:

$$2Ca(PO_3)_2 + H_2O \rightarrow Ca_2P_2O_7 + 2HPO_3\uparrow$$

Fig. 9 shows the temperature dependence of shrinkage for ceramic materials.

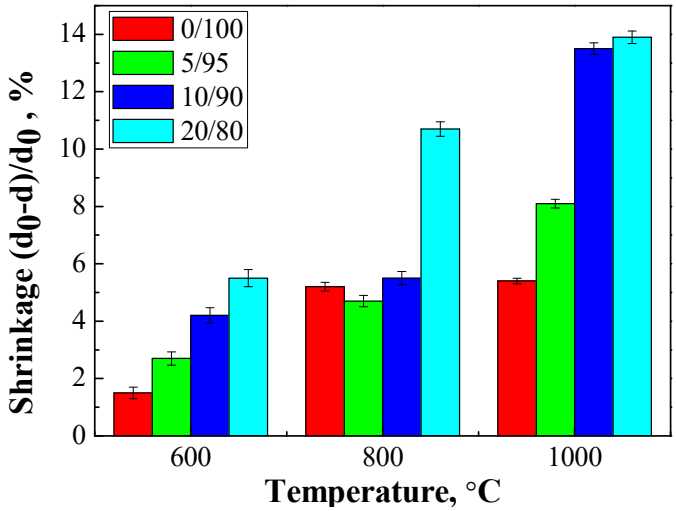

Fig. 9. Shrinkage of ceramic materials, with weight ratio of: a) $Ca(PO_3)_2/Ca_2P_2O_7$=0/100; b) $Ca(PO_3)_2/Ca_2P_2O_7$=5/95, c) $Ca(PO_3)_2/Ca_2P_2O_7$=10/90, d) $Ca(PO_3)_2/Ca_2P_2O_7$=20/80 in the range of 600-1000 °C temperatures.

Composition 20/80 gives the greatest shrinkage at all temperatures, gradually increasing from 600 to 1000 °C, while composition 10/90 gives a sharp increase in shrinkage to 1000 °C, which probably is associated with a large amount of liquid phase and recrystallization.

The strength of ceramic matrices obtained by annealing a cement stone at 1000°C exceeds several times the unannealed cement stone of compositions 20/80 and 10/90, while compositions 0/100 and 5/95 after annealing have lower strength characteristics than before annealing (**Fig. 10**).

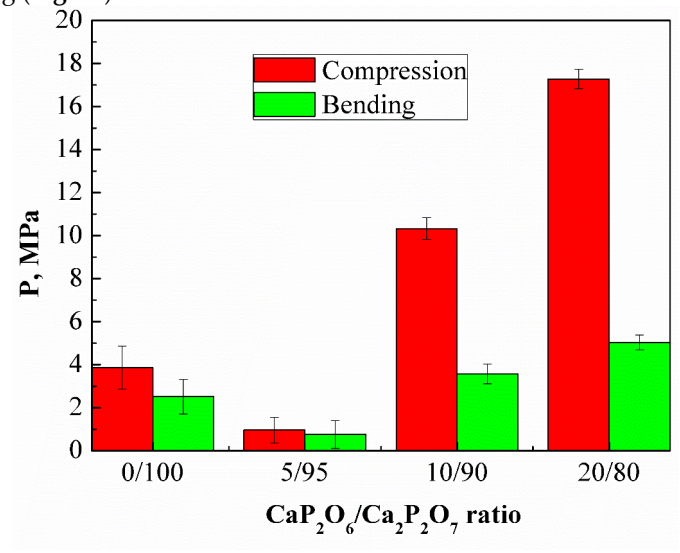

Preprints (www.preprints.org) | NOT PEER-REVIEWED | Posted: 5 July 2022 doi:10.20944/preprints202207.0073.v1

Fig. 10. Compressive and bending strengths of samples with weight ratio of: a) $Ca(PO_3)_2/Ca_2P_2O_7$ = 0/100; b) $Ca(PO_3)_2/Ca_2P_2O_7$ = 5/95, c) $Ca(PO_3)_2/Ca_2P_2O_7$ = 10/90, d) $Ca(PO_3)_2/Ca_2P_2O_7$ = 20/80 after annealing at a temperature of 1000 °C

It is likely that an increase in the amount of polyphosphate due to excess MCPM in the initial mixture leads to liquid-phase sintering, improving the sintering ability and homogeneity of the ceramics, leading to an increase in mechanical strength.

SEM images of the obtained samples after annealing at 1000 °C are shown in **Fig. 11.**

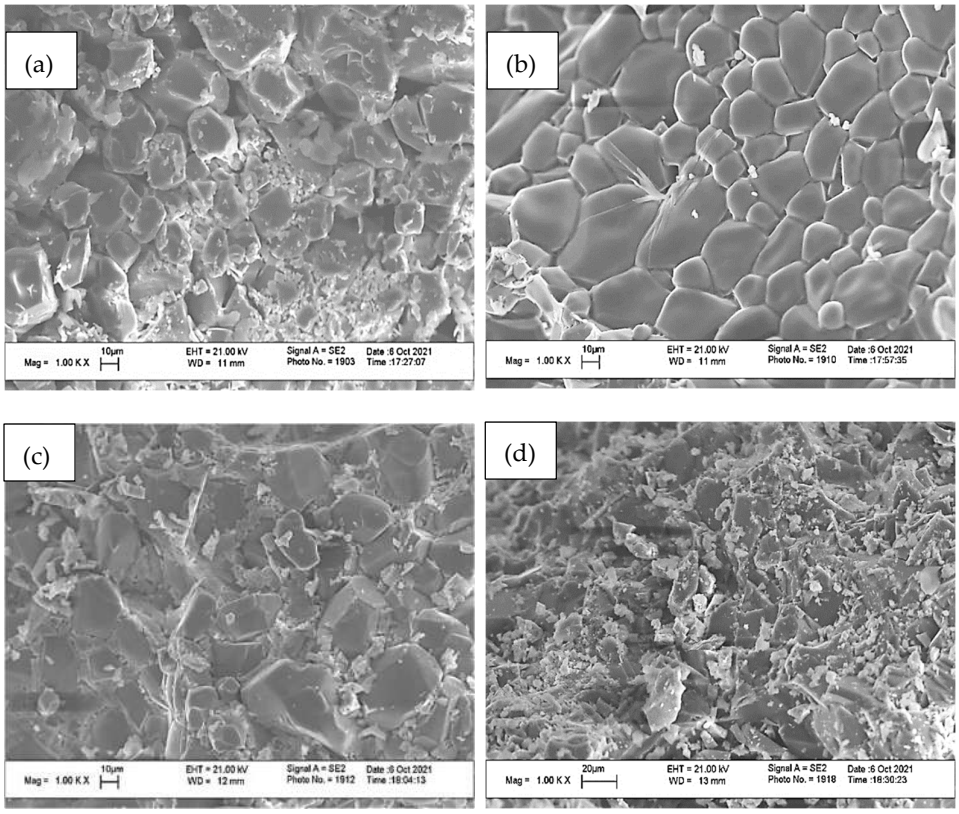

Fig. 11. SEM images of the ceramic materials, with weight ratio of: a) $Ca(PO_3)_2/Ca_2P_2O_7$ =0/100; b) $Ca(PO_3)_2/Ca_2P_2O_7$=5/95, c) $Ca(PO_3)_2/Ca_2P_2O_7$=10/90, d) $Ca(PO_3)_2/Ca_2P_2O_7$=20/80 at a temperature of 1000 °C

The microstructure of a 0/100 ceramic material is represented by prismatic calcium pyrophosphate crystals of various sizes. Sample of ceramic material 5/95 is represented by prismatic crystals of calcium pyrophosphate with smoothed edges, which is probably due to the melting above 950°C of calcium polyphosphate formed by heating excess MCPM to temperatures above 500°C. The decomposition of $Ca(PO_3)_2$, which initially forms a liquid phase, is observed in micrographs of compositions 10/95 and 20/80, where small crystals of calcium pyrophosphate crystallize in the intercrystalline space of calcium pyrophosphate. The 20/80 composition is distinguished by smaller crystals.

Preprints (www.preprints.org) | NOT PEER-REVIEWED | Posted: 5 July 2022 doi:10.20944/preprints202207.0073.v1

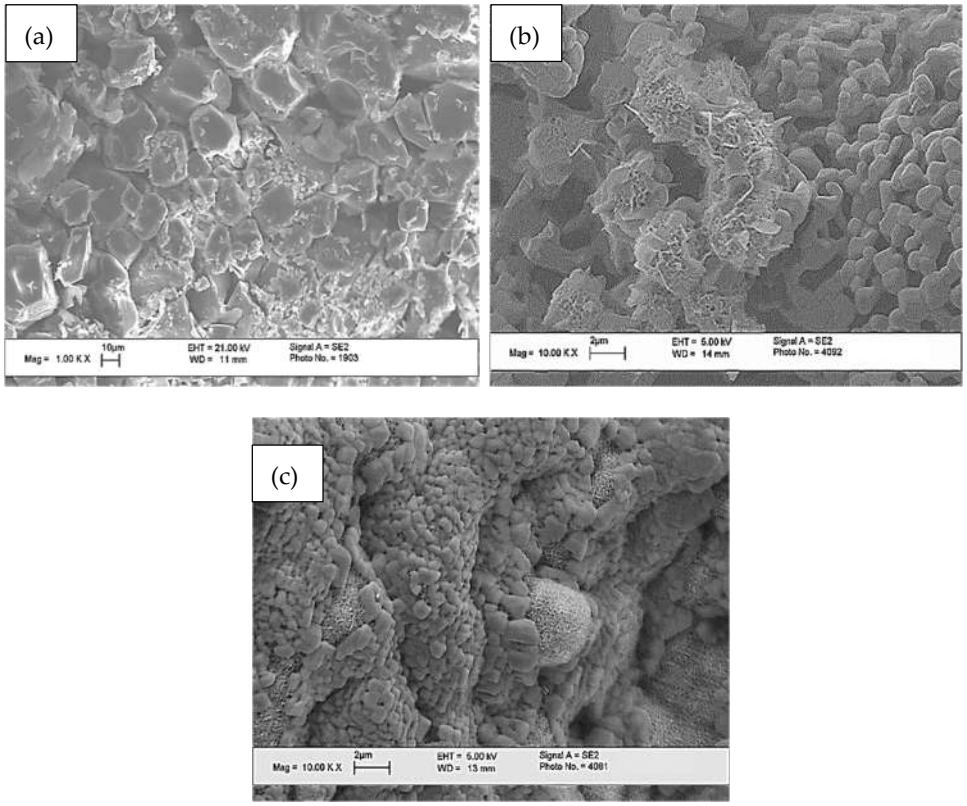

Fig. 12. SEM images of the surface of ceramic samples based on β-$Ca_2P_2O_7$ before (a), during (b) and after mineralization for 7 days (c) of the model medium SBF

When studying the behavior of porous ceramic materials, in a solution that simulates the composition of interstitial fluid, after 1 and 7 days, the formation of a characteristic openwork layer of apatite was observed, as can be seen from SEM images (**Fig. 12**). The results of SBF sedimentation studies confirm that porous ceramic materials contribute to the crystallization of apatite from supersaturated solutions - analogues of interstitial fluids.

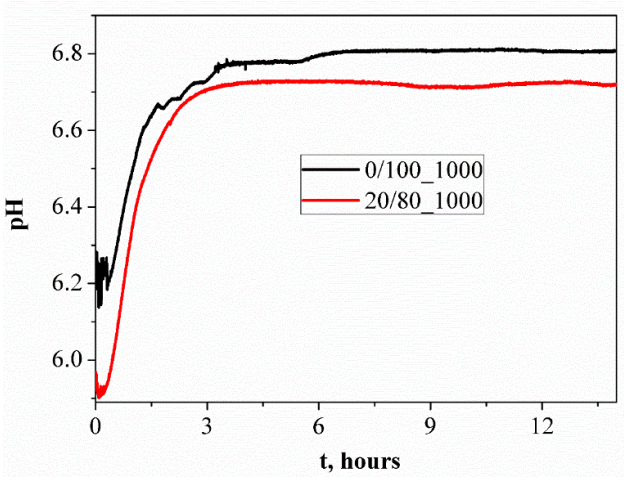

Fig. 13. pH - metering of aqueous solutions of ceramic samples, fired at 1000 °C

According to the results of pH - measurements of aqueous solutions of the samples, the pure phase of calcium pyrophosphate (CaP_2O_6/$Ca_2P_2O_7$ = 0/100) has a virtually neutral pH level (**Fig. 13**). As the calcium polyphosphate phase content increases, a slight acidification of the solution in the samples occurs. pH-measurements of the obtained materials were conducted using their aqueous solutions with a pH of 6.8, which falls in the natural

Preprints (www.preprints.org) | NOT PEER-REVIEWED | Posted: 5 July 2022 doi:10.20944/preprints202207.0073.v1

pH (6.4 - 8.4) range of the human body. Thus, the pH of the resulting materials is acceptable to the human body. In **Fig. 14** was shown the in vivo test results of ceramic samples based on β – $Ca_2P_2O_7$ which annealed at 1000 °C.

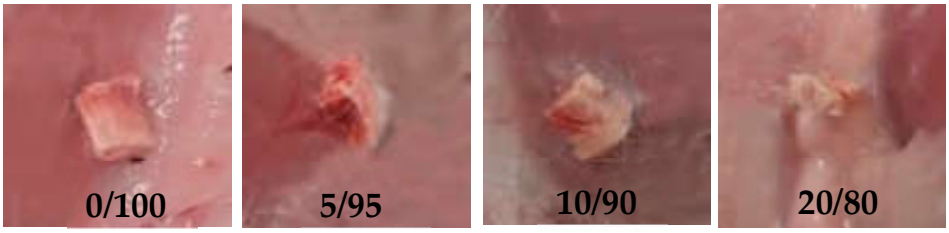

Fig. 14. Images of a rat after implantation

The best results of biocompatibility are possessed by implants consisting of calcium pyrophosphate / calcium polyphosphate in ratios of 20/80 and 10/90 (Table 2). In these prototypes, thin, mature capsules are formed with densely spaced and parallel oriented collagen fibers and few fibroblasts between them, with minimal inflammatory infiltration and vascularization. Less mature capsules are formed around implants of a different composition, in which the macrophage lining in the inner layer is partially retained and moderate lympho-macrophage infiltration and vascularization are noted.

Samples which were shown in the **Fig. 15** are practical confirmation of the idea of slowing down the setting time allowed for layer-by-layer printing.

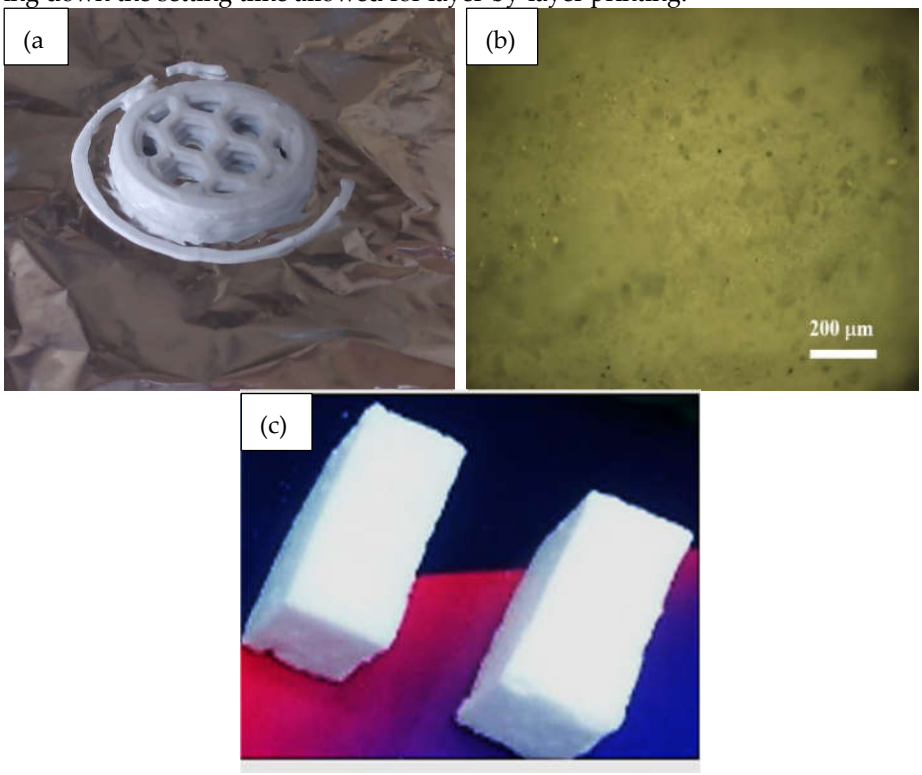

Fig. 15. Samples formed by highly concentrated hardening suspensions:
a) extrusion 3D-printing, b) optical image of samples, c) shaping the girders

Fig. 15 a shows the samples based on calcium citrate and MCPM formed by extrusion 3D-printing. The surface of ceramic materials can be seen by optical microscope (Fig. 15 b). Microstructure of obtained ceramic materials via 3D-printing shows a uniform porous morphology. Fig. 15 c represents the girders shaped from calcium citrate and MCPM, obtained by casting into appropriate molds at room temperature.

 doi:10.20944/preprints202207.0073.v1

4. Conclusions

Ceramic materials based on calcium pyrophosphate $Ca_2P_2O_7$ were obtained by annealing cement stone based on powder mixtures of calcium citrate tetrahydrate $Ca_3(C_6H_5O_7)_2{\cdot}4H_2O$ and monocalcium phosphate monohydrate (MCPM) $Ca(H_2PO_4)_2{\cdot}H_2O$ taken in molar ratio of 1:3. A lower melting phase of $Ca(PO_3)_2$ forming from an excess of $Ca(H_2PO_4)_2{\cdot}H_2O$ makes it possible to reduce the annealing temperature of ceramics.

The plastic strength of highly concentrated suspensions based on monocalcium phosphate monohydrate and calcium citrate tetrahydrate depends on the composition and hardening process, due to the formation of brushite/monetite phases. The increasing of plastic strength is associated with the process of hardening of cement solutions and formation of cement stone.

The use of calcium citrate tetrahydrate can significantly reduce the rate of formation of brushite, which makes it possible to use highly concentrated suspensions for extrusion 3D printing. Highly concentrated suspensions set and harden with the formation of cement stone, maintaining the shape of the matrix. Annealing of cement stone is accompanied by the following processes: the formation of the calcium pyrophosphate phase as a result of thermal transformation of calcium hydrophosphates with a Ca/P ratio of 1; the conversion of unreacted chemical binding of calcium citrate to calcium carbonate, and MCPM to calcium polyphosphate; the formation of the calcium pyrophosphate phase as a result of a heterophasic reaction of calcium carbonate and calcium polyphosphate.

In vivo tests of the obtained materials based on $\beta - Ca_2P_2O_7$ suggest that they can be recommended for regenerative treatments for bone defects.

Author Contributions: Conceptualization, O.T. (Otabek Toshev) and M.K. (Maksim Kaimonov); Methodology, T.S. (Tatiana Safronova); Investigation, O.T., T.S. (Tatiana Safronova), T.S. (Tatiana Shatalova), Yu. L. (Yulia Lukina), E.K. (Elena Klimashina) and K.M. (Konstantin Malyutin); Visualization, T.S. (Tatiana Shatalova); Writing—original draft, O.T. and T.S. (Tatiana Safronova); Writing—review & editing, O.T.; Supervision, T.S. (Tatiana Safronova); Project administration, T.S. (Tatiana Safronova). All authors have read and agreed to the published version of the manuscript.

Funding: This work was carried out with financial support from the Russian Foundation for Basic Research (RFBR) (grant No. 20-03-00550 A).

Institutional Review Board Statement: The animal study protocol was approved by the Institutional Review Board (or Ethics Committee) of National Medical Research Center for Traumatology and Orthopedics named after N.N. Priorov, Ministry of Health of the Russian Federation (protocol code 005, date of approval 12.05.2021).

Acknowledgments: This work was carried out using equipment purchased at the expense of the Moscow University Development Program.

Conflicts of Interest: The authors declare that they have no known competing financial interests or personal relationships that could have appeared to influence the work reported in this paper.

References

1. Kucko, N.W., Herber, R.-P., Leeuwenburgh, S.C.G., Jansen, J.A. Calcium Phosphate Bioceramics and Cements. *Principles of Regenerative Medicine,* **2019**; *3(34)*, 591–611.
2. Salimi, E. Functionally graded calcium phosphate bioceramics: An overview of preparation and properties. *Ceram. Int.,* **2020,** *46,* 19664–19668.
3. Safronova, T.V. Inorganic Materials for Regenerative Medicine. *Inorg. Mater.,* **2021,** *57(5),* 443–474.
4. Safronova, T.V., Kurbatova, S.A., Shatalova, T.B., Knotko, A.V., Yevdokimov, P.V., Putlyayev, V.I. Calcium pyrophosphate powder for production of bioceramics synthesized from pyrophosphoric acid and calcium acetate. *Inorg. Mater.: Appl. Res.,* **2017,** *8(1),* 118–125.
5. Safronova, T.V., Shatalova, T.B., Filippov, Y.Y., Krut'ko, V.K., Musskaya, O.N., Safronov, A.S., Toshev, O.U. Ceramics in the Ca2P2O7–Ca(PO3)2 system obtained by annealing of the samples made from hardening mixtures based on calcium citrate tetrahydrate and monocalcium phosphate monohydrate. *Inorg. Mater.: Appl. Res.,* **2020,** *11(4),* 777–786.
6. Metsger, D.S., Driskell, T.D., Paulsrud, J.R. Tricalcium phosphate ceramic — a resorbable bone implant: review and current status. *J. Am. Dent. Assoc*., **1982**, *105(6),* 1035–1038.

7. Daculsi, G. Biphasic calcium phosphate concept applied to artificial bone, implant coating and injectable bone substitute. *Biomaterials*, **1998**, *19(16),* 1473—1478.
8. Valletregi, M. Calcium phosphates as substitution of bone tissues. *Progress in solid state chemistry*, **2004**, *32(1-2),* 1–31.
9. Habraken, W., Habibovic, P., Epple, M., Bohner, M. Calcium phosphates in biomedical applications: materials for the future? *Materials Today*, **2016,** *19(2*), 69–87.
10. Canillas, M., Pena, P., de Aza A.H., Rodriguez, M.A. Calcium phosphates for biomedical applications. *Boletin de La Sociedad Espanola de Ceramica y Vidrio*, **2017**, *56(3)*, 91–112.
11. Bouler, J.M., Pilet, P., Gauthier, O., Verron, E. Biphasic calcium phosphate ceramics for bone reconstruction: A review of biological response. *Acta Biomaterialia*, **2017**, 53, 1–12.
12. Jeong, J., Kim, J.H., Shim, J.H., Hwang, N.S., Heo, C.Y. Bioactive calcium phosphate materials and applications in bone regeneration. *Biomaterials Research*, **2019**, *23(1)*, 1-11.
13. Safronova, T.V., Putlyaev, V.I. Powder systems for calcium phosphate ceramics. *Inorg. Mater*., **2017**, *53(1)*, 17–26.
14. Hurle, K., Oliveira, J.M., Reis, R.L., Pina, S., Goetz-Neunhoeffer, F. Ion-doped Brushite Cements for Bone Regeneration. *Acta Biomaterialia*, **2021**, *123,* 51-71.
15. Boanini, E., Silingardi, F., Gazzano, M., Bigi, A. Synthesis and Hydrolysis of Brushite (DCPD): The Role of Ionic Substitution. *Cryst. Growth Des*. **2021**, *21,* 1689−1697.
16. Zhou, H., Yang, L., Gbureck, U., Bhaduri, S.B., Sikder, P. Monetite, an important calcium phosphate compound–Its synthesis, properties and applications in orthopedics. *Acta Biomaterialia*, **2021**, *127*, 41–55.
17. Motameni, A., Alshemary, A.Z., Evisa, Z. A review of synthesis methods, properties and use of monetite cements as filler for bone defects. *Ceram. Int*., **2021**, *47,* 13245–13256.
18. Safronova, T.V., Putlyaev, V.I., Kurbatova, S.A., Shatalova, T.B., Larionov, D.S., Kozlov, D.A., Evdokimov, P.V. Properties of amorphous calcium pyrophosphate powder synthesized via ion exchange for the preparation of bioceramics. *Inorg. Mater.,* **2015,** *51,* 1177–1184.
19. Lee, J.H., Chang, B.-S., Jeung, U.-O., Park, K.-W., Kim, M.-S., Lee, C.-K. The first clinical trial of beta-calcium pyrophosphate as a novel bone graft extender in instrumented posterolateral lumbar fusion. *Clinics in orthopedic surgery*, **2011**, *3(3),* 238.
20. Safronova, T.V., Putlyaev, V.I., Ivanov, V.K., Knot'ko, A.V., Shatalova, T.B. Powders mixtures based on ammonium hydrophosphate and calcium carbonate for preparation of biocompatible porous ceramic in the CaO–P2O5 system. *Refractories and Industrial Ceramics*, **2016,** *56(5),* 502-509.
21. Safronova, T.V., Putlayev, V.I., Bessonov, K.A., Ivanov, V.K., Ceramics based on calcium pyrophosphate nanopowders. *Processing and Application of Ceramics*, **2013**, *7(1)*, 9–14.
22. Lin, F.-H., Liao, C.-J., Chen, K.S., Sun, J.-S., Liu, H.-C. Degradation behaviour of a new bioceramic: Ca2P207 with addition of Na4P2O7•10H2O. *Biomaterials*, **1997**, *18(13)*, 915–921.
23. Webb, N.C. The crystal structure of β-Ca2P2O7. *Acta Cryst.,* **1966**, *21(6)*, 942–948.
24. Weil, M., Puchberger, M., Schmedt auf der Günne, J., Weber, J. Synthesis, crystal structure, and characterization (Vibrational and Solid-State31P MAS NMR Spectroscopy) of the high-temperature modification of calciumcatena-polyphosphate(V*). Chemistry of Materials*, **2007**, *19(21),* 5067–5073.
25. Kondrashenko, E.V., Kondrashenko, V.I., Kudryavtseva, V.D., Grebennikov, D.A., Semak, A.V. Opredeleniye plasticheskoy prochnosti rastvornykh i betonnykh smesey, Library of National Technical University "*Kharkiv Polytechnic Institute*", **2012**.
26. Mirtchi, A.A, Lemaitre, J., Terao, N. Calcium phosphate cements: study of the beta-tricalcium phosphate – monocalcium phosphate system, *Biomaterials*, **1989,** *10(7),* 475– 480.
27. Hill, W.L., Hendricks, S.B. Composition and properties of superphosphate: Calcium phosphate and calcium sulfate constituents as shown by chemical and x-Ray diffraction Analysis. *Industrial & Engineering Chemistry*, **1936,** *28(4),* 440–447.
28. Schrödter, K., Bettermann, G., Staffel, T., Wahl, F., Klein, T., Hofmann, T. Phosphoric acid and phosphates. *Ullmann's Encyclopedia of Industrial Chemistry*, **2008,** *26(7),* 679-724.
29. Rothammel, W., Burzlaff, H., Specht, R. Structure of calcium metaphosphate Ca(PO3)2. *Acta Crystallographica Section C Crystal Structure Communications,* **1989,** *45(4),* 551–553.